Switchable Ytterbium Fiber Laser Based on a Symmetrical Long-Period Fiber Grating
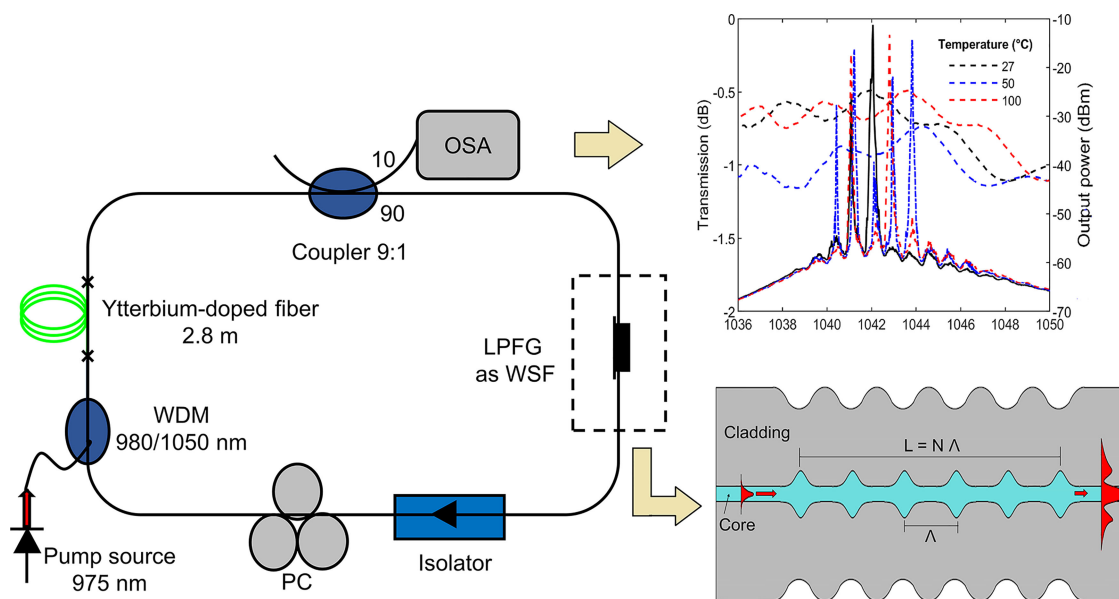
Erika C. Silva-Alvarado
Alejandro Martinez-Ríos
Luis M. Ledesma-Carrillo
Daniel Jauregui-Vazquez
Guillermo Salceda-Delgado
Teresa Elena Porraz-Culebro
Javier Antonio Martin Vela
Juan Manuel Sierra-Hernandez

Switchable Ytterbium Fiber Laser Based on a Symmetrical Long-Period Fiber Grating

Erika C. Silva-Alvarado,[1] **Alejandro Martinez-Ríos** ⓘ**,**[2]
Luis M. Ledesma-Carrillo,[3] **Daniel Jauregui-Vazquez,**[1]
Guillermo Salceda-Delgado,[4] **Teresa Elena Porraz-Culebro** ⓘ**,**[2]
Javier Antonio Martin Vela ⓘ**,**[1]
and Juan Manuel Sierra-Hernandez ⓘ[1]

[1]Departamento de Ingeniería Electrónica, Campus Irapuato-Salamanca, Universidad de Guanajuato, Salamanca, Gto C.P. 36885, México
[2]Centro de Investigaciones en Óptica, León Guanajuato C.P. 37105, México
[3]Departamento de Estudios Multidisciplinarios, Campus Irapuato-Salamanca, Universidad de Guanajuato, Yuriria, Guanajuato C.P. 38940, México
[4]Facultad de Ciencias Físico Matemáticas, Universidad Autónoma de Nuevo León, San Nicolas de los Garza 66455, México

Abstract: In this study, a switchable ytterbium-doped fiber laser based on symmetrical long-period fiber grating (LPFG) is presented. The LPFG is used as a wavelength-selective filter (WSF). Utilizing this WSF, the laser can emit one, two, or multiple stable output beams by adjusting the temperature on the LPFG from 20 °C to 600 °C. In addition, switching is also possible by adjusting the curvature of the LPFG from 0.399 to 0.709 m^{-1}. The symmetrical LPFG was fabricated by combining the cladding shaping with the thermal core expansion techniques by using a CO_2-laser LZM-100 glass-processing system. The experimental results show a side-mode suppression ratio (SMSR) of 49 dB and a linewidth of 0.06 nm, within the range from 1038 to 1080 nm. In conclusion, the main achievement of this switchable laser is the high SMSR and stable output for high values of temperature, using a repeatable, simple, easy construction, and cost-effective laser tuning technique.

Index Terms: Ytterbium fiber laser, long period fiber grating (LPFG), switchable, CO_2-laser glass processing system.

1. Introduction

Continuous-Wave fiber lasers have been widely used as light sources due to their unique properties such as high output power [1]–[4], high SMSR [5]–[7], narrow linewidth [8]–[11], high stability at room temperature [12]–[15] and low fabrication cost [16]–[18]. Switchable multi-wavelength fiber lasers (MWFL) are desirable because of their ability to emit single, double, or multiple line emissions in a wavelength range [19], [20]. In effect, the capacity of switching the number of laser lines and their wavelength is very useful in a broad field of applications, such as biomedical technology [21], [22] sensing [23], [24], spectroscopy [25], dense wavelength division multiplexing [26], optical communications [27], and microwave photonics systems [28]. An essential element for switchable

MWFL is a wavelength selective filter (WSF) inserted in the laser cavity. Several devices have been proposed as WSF, such as a parallel-structured Lyot filter [29], fiber Bragg grating (FBG) [30] or Sagnac loop mirror [31]–[34]. On one hand, to implement a Lyot filter a large fiber structure is required. A Sagnac loop mirror requires external components besides a section of polarization-maintaining optical fiber. In an arrangement based on FBGs, the number of switchable wavelengths requires an equal amount of FBGs [30]. On the other hand, a remarkable variety of WSFs are based on interferometers such as Mach-Zehnder [35]–[38], Fabry-Perot [39] or Michelson [40], [41] and long-period fiber grating (LPFG) [42]. In all the above studies, a crucial challenge to achieve a switchable MWFL operation is given by the strong mode competition and unstable laser output [43], [44] caused by the homogeneous gain broadening of the rare-earth doped fiber gain medium [45]. Improving these aspects, ytterbium-doped fiber lasers (YDFLs) have been used in industrial or medical applications [46] because of its attractive features, including: an appreciable broader lasing wavelength range of 970-1200 nm [47], [48] and a better pump slope efficiency [49] due in large part to the absence of various competing processes present in other rare-earth dopants [50].

For these reasons, switchable multi-wavelength YDFL has been widely investigated. In [51] a switchable dual-wavelength YDFL using an arrayed waveguide grating together with an optical channel selector as WSF, achieved a SMSR of ∼60 dB, with 0.47 dB of stability. In [52], an Yb-doped MZI used as WSF, resulted in a laser with a SMSR of 40 dB, a linewidth of 0.07nm, and stability of 1 dB during 30 minutes of testing. In [53] a non-adiabatic microfiber Mach-Zehnder interferometer was used as a WSF, obtaining a laser with a SMSR of 53 dB, a linewidth of 0.01 nm, and stability 0.6 dB during 20 minutes of testing. Recently, in [48], the switchable emission was controlled by bending a bitaper MZI, obtaining a SMSR of about 32 dB.

An alternative approach is using a LPFG as the wavelength-selective filter, as reported in [42]. Here, a three-wavelength lasing operation was obtained at 1081.5, 1090.5, and 1100.7 nm, with linewidth around 1 nm. Moreover, the net laser gain in the cavity is changed by adjusting the twist rate and the pressure on the mechanical-induced LPFG (MLPFG). However, the disadvantages of MLPFG are high sensitivity to ambient temperature, and high insertion losses, often in the order of 0.2 - 0.3 dB [54]. Another laser based on a phase-shifted LPFG is described in [55], in which dual and triple wavelength lines, with a SMSR of 40 dB were obtained.

In [56] was experimentally demonstrate the selection of the operating wavelength of a cladding-pumped YDFL using LPFGs made of CO2-laser inscription technique, achieving 1080 − 1100 nm of wavelength range, which can be extended depending on the grating used and the Yb-doped fiber length and the coupler output port.

Generally, LPFGs induce an asymmetrical and polarization-dependent coupling between core and cladding modes, due to the no uniform absorption energy on the incident side of the fiber in their fabrication process [57]. In the case of LPFGs fabricated with CO2 laser, the birefringence increases mainly by azimuthal asymmetry of the laser exposure, since the fabrication typically adopts the surface deformation [58]. However, LPFGs fabricated with a CO2-laser LZM-100 glass-processing system, which provides uniform heat deposition, allows the construction of axially symmetric LPFGs [59], [60]. It has been demonstrated that the polarization-dependent loss (PDL) of the axially symmetric LPFGs can be reduced to a level comparable to that of the SMF fiber [58].

In this paper, we report a switchable multi-wavelength YDFL using a WSF based on symmetrical LPFG. Adjusting the temperature of the symmetrical LPFG, multiple lines can be switched over the range from 1038 to 1080 nm. SMSRs of around 50 dB and linewidths of around 0.06 nm have been obtained. Also, the proposed method shows to have wavelength emission stability with output power fluctuations below to 0.14 dB. In addition, switchable operation is also possible adjusting a curvature of the LPFG from 0.399 to 0.709 m^{-1}.

2. Experimental Setup

Fig. 1 shows the experimental setup of the switchable multiwavelength YDFL. Here, a 975 nm laser semiconductor diode (Qphotonics, model QFBGLD-980-350) is used as the pumping source toward a 980 nm/1050 nm wavelength division multiplexer (WDM), launching the pumping power
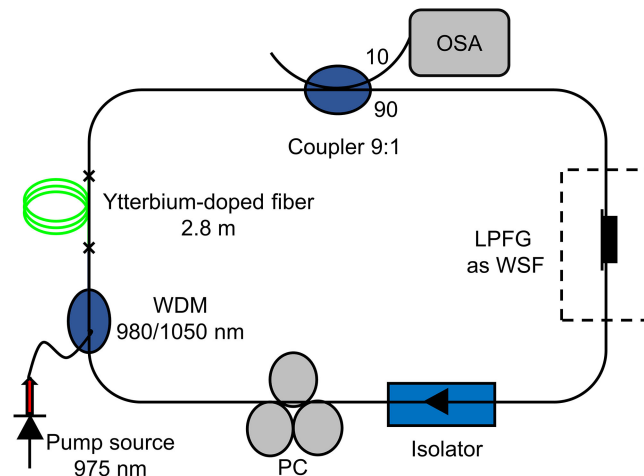
Fig. 1. Experimental setup of the proposed switchable YDFL.

into the ring laser cavity. The active medium is a 2.8 m segment of ytterbium-doped fiber (Liekki, model YB1200-10/125DC) with a concentration of about 9×10^{19} ions/cm^3 [61], the nominal peak cladding absorption of the fiber at 976 nm is 7.4 dB/m, and the core diameter is about 10 mu;m. The ytterbium-doped fiber length was determined experimentally to maximize the amplified spontaneous emission. Next, we inserted into the ring cavity a 2×2 single-mode fiber coupler with a 90:10 ratio of two outputs, and with an adequate wavelength range operation for the YDFL emissions. The 10% output port is used as the laser output, and it is connected to an optical spectrum analyzer (Yokogawa, ModelAQ6370B) with a resolution of 0.02 nm. The 90% output port was placed toward the LPFG.

The LPFG is used as a WSF for the switchable YDFL. The WSF in the ring cavity provides different advantages, such as cleaning the shape of the lasing spectrum, balancing the losses induced by the homogeneous broadening in the ytterbium-doped fiber, and stabilizing the laser operation. An optical isolator was placed after the WSF, to ensure unidirectional light propagation, protecting the pumping source from back reflection and preventing spatial hole burning in the doped fiber, which may cause system instability [17]. The isolator output port was then connected to the polarization controller (PC) to rotate the polarization states, allowing continuous adjustment of the birefringence inside the ring cavity, and switching the number of wavelength peaks in the laser output spectrum. The PC output is spliced to the WDM, closing the ring laser cavity. Finally, the total ring cavity length is less than 15 m.

3. LPFG Fabrication and Operation Principle

The fabrication of the symmetrical LPFG was implemented by a programmable routine in a CO2-laser glass processing system (LZM-100 from AFL) to create several tapering points separated by a constant distance (period). Here, the CO2-laser beam is directed to a beam splitter by a mirror to form two diverging beams, which are reflected onto the entire surface of a conventional single-mode fiber (SMF-28), as it is depicted in Fig. 2(a).

First, the CO2 laser power was applied for 120 ms on the SMF-28, while the two motorized holders, shown in Fig. 2(b), travel with different velocities to generate a small tapered section in the fiber. After that, both motorized holders move at the same speed for a distance corresponding to the LPFG period. Then the process is repeated a determined number of times to generate a periodical structure composed of equally separated tapering points in a total length of around 21 mm.

Further explanation about the fabrication method of the symmetrical LPFG can be found in [60]. At each tapered waist, the cladding diameter is reduced whereas the core is expanded, due to the
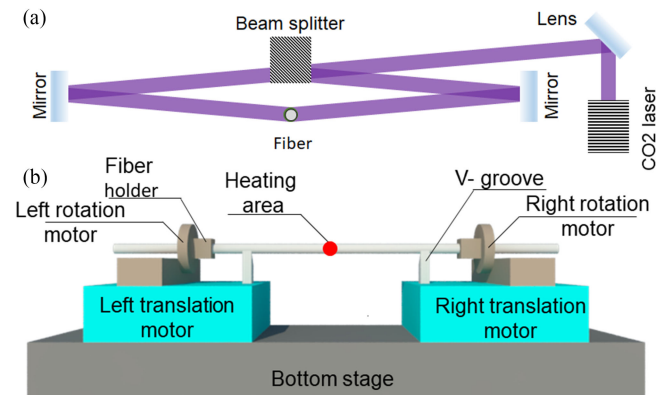
Fig. 2. (a) The heating deposition system, based on a CO2-laser and a beam splitter, for the LPFG fabrication technique. (b) Scheme of LZM-100 glass processing system.
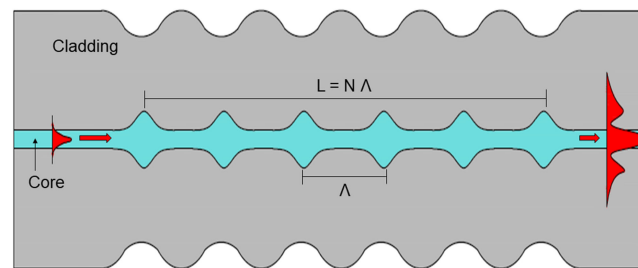

Fig. 3. Schematic diagram of the symmetrical LPFG, with a periodic tapered cladding zone and a core expansion.

diffusion of dopants in the core fiber during the CO2 laser heating, obtaining a LPFG geometry not only longitudinally but also axially symmetric, as it is depicted in Fig. 3. The length of the LPFG is $L = N\Lambda$, where N is the number of tapers and Λ is the period of the perturbation [60].

Furthermore, due to the thermal expansion of the core, the mode field diameter (MFD) is also locally expanded at each taper location [62]. The germanium in the core is diffused toward the cladding [63] increasing the MFD as is shown in [64], in which were observed two bright points of irradiation on an axial cut-off in the middle of the thermally-expanded core, similar to LP11 mode. Then, due to the micro-tapering of the cladding, the evanescent portion of the electromagnetic field is spreading out to interact with the environment close to the surface of the fiber, enhancing the sensitivity. Finally, at the end of each expanded core region, the fiber returns to its original MFD, exciting the high-order cladding modes LP0m, as is observed in [60], [65]. These modes have axial symmetry, and therefore, the coupling of the fundamental core mode and the cladding modes in this symmetrical LPFG allows to create a wavelength selective fiber [66].

Compared to conventional LPFGs, the average temperature tuning efficiency of the symmetrical LPFG is greatly improved [67]. The combination of the geometrical change induced by the tapering and core expansion produces changes in the effective refractive index of the fiber, mainly due to the frozen-in viscoelasticity and mechanical stress. Where the core refractive index decreases, the cladding refractive index increases [60]. This axisymmetric periodic perturbation of the fiber has the advantage of achieving symmetric coupling of energy from the core mode towards cladding modes [5]. The symmetrical LPFG was chosen as the WSF of the switchable multiwavelength YDFL. In our experiment, a symmetric LPFG with 35 periods of $\Lambda = 600\mu$m with a total length of 21 mm was manufactured.
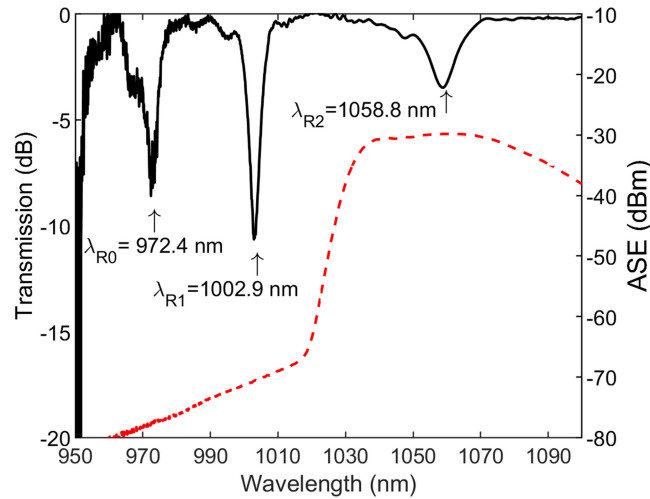
Fig. 4. The output spectrum of symmetric LPFG at room temperature (20 °C).

An initial characterization of the symmetric LPFG was done at room temperature (20°C), then the source spectrum was subtracted from the LPFG spectrum, resulting in the transmission spectrum of the LPFG showed in Fig. 4. Here, three notches are observed at the resonance wavelengths of $\lambda_{R0} = 972.4$ nm, $\lambda_{R1} = 1002.9$ nm, and $\lambda_{R2} = 1058.8$ nm, with a maximum notch depth of 9, 11 and 4 dB, respectively. Here, the high noise presented in the depth at λ_{R0} is due to the low gain of the YDF below 1000 nm. Each resonance wavelength λ_R is associated with the coupling of the fundamental core mode to a specific cladding mode, by the resonance condition (1) [68] :

$$\lambda_R = \; \wedge \left(n_{eff}^{co} - n_{eff}^{cl} \right) \tag{1}$$

Where n_{eff}^{co} and n_{eff}^{cl} are wavelength-dependent effective indices of the fundamental core more and the cladding mode, respectively. It is known that n_{eff}^{cl} decreases when the cladding mode order increases [69], resulting in a higher effective index difference between the LP01 core mode and the LP0m cladding modes. Since the resonance wavelength is proportional to the effective index difference between core and cladding mode (Eq. (1)) the separation between λ_{R0} and λ_{R1} is shorter than the separation between λ_{R1} and λ_{R2} (Fig. 4). The modal coupling strength is weaker for the higher-order cladding mode LP0m, because of its more significant power fraction outside the fiber core [69]. This can explain why the depth at λ_{R1} is more pronounced than at λ_{R2}. Given the transmission spectrum, there are two pass bands where we can expect the laser emission at room temperature: the first one for wavelengths between 1002.9 nm and 1058.8 nm, where the ASE is higher, and the second one above $\lambda_{R2} = 1058.8$ nm.

4. Experimental Results

We analyze the effect of the temperature upon the LPFG when used as WSF; Fig. 5 shows the wide range temperature tuning of the transmission spectrum of the symmetrical LPFG. Here, the resonant wavelength λ_{R1} shifts from 1002.9 nm (27°C, black line) to 1032.1 nm (600°C, green line) and λ_{R2} shifts from 1058.8 nm (27°C, black line) to 1086 nm (600°C, green line). Moreover, we can observe that in the case of λ_{R1} the depth increases when shifting from 1058.8 nm (27°C, black line) to 1086 nm (600°C, green line). Nevertheless, since λ_{R0} remains below 1000 nm, it is difficult to achieve lasing, therefore, λ_{R0} was not analyzed.

The shifting of λ_R toward longer wavelengths as the temperature increases can be explained with an increment of the effective index difference between the core mode and the cladding modes in
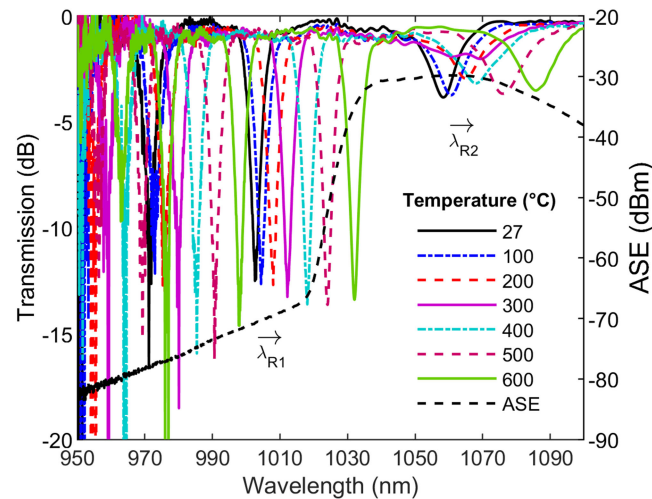
Fig. 5. The output spectrum of symmetric LPFG versus temperature.

the LPFG as the temperature increases, as already reported in [70].

$$\frac{d\lambda_R}{dT} = \gamma \lambda_R \left(\alpha + \frac{\xi_{co} n_{eff}^{co} - \xi_{cl} n_{eff}^{cl,m}}{n_{eff}^{co} - n_{eff}^{cl}} \right) \tag{2}$$

where ξ_{co}, and ξ_{cl} are the thermo-optic coefficients of the core and cladding materials, respectively, α is the thermal expansion coefficient of the fiber, and γ is the waveguide dispersion and is defined by (3):

$$\gamma = \frac{n_{eff}^{co} - n_{eff}^{cl}}{n_g^{co} - n_g^{cl,m}} \tag{3}$$

Where $n_g^{co} - n_g^{cl,m}$ is the group index difference between the core and the m-th cladding mode and exhibits a positive slope at the 0.8–2.0 μm wavelength range for the first cladding modes [70]. In general, for silica-based fiber, α is lower than the thermo-optic coefficient term that could be higher than zero. Since $n_{eff}^{co} - n_{eff}^{cl}$ is positive, the resonant wavelengths of the symmetrical LPFG shifts toward longer wavelengths as the temperature is increased [70].

On the other hand, the effective refractive indices for the core and cladding modes increase with the temperature, but decrease at higher wavelengths [71]. The first effect prevails at λ_{R2}, making stronger the coupling at higher temperatures, meanwhile both effects alter the notch depth of λ_{R2}.

The sensitivity of the symmetrical LPFG under temperature variation was calculated with linear regression of each resonant wavelength observed in Fig. 5 vs. temperature, obtaining $\frac{d\lambda_{R1}}{dT} \approx$ 0.0507 nm/°C and $\frac{d\lambda_{R2}}{dT} \approx$ 0.0499 nm/°C, from 27°C to 600°C (Fig. 6).

4.1 Single Laser Emission

It is widely known that the presence of a wavelength selective filter in a fiber ring laser avoid the gain competition due to the homogeneous broadening of the ytterbium-doped fiber [24]. In our case the symmetrical LPFG was used as a WSF element. For this experimental analysis at room temperature, we set the laser diode at the saturation power of the YDF (150 mW), and the sample interval of signal acquisition by the optical spectral analyzer (OSA) at 0.02 nm. To obtain laser emission (Fig. 7, blue line), it is necessary to achieve the balance between the homogeneous gain broadening of the ytterbium-doped fiber (Fig. 7, red line) and the losses produced by the WSF (Fig. 7, black line). It can be noticed that for single emission regime, attenuation band with resonant
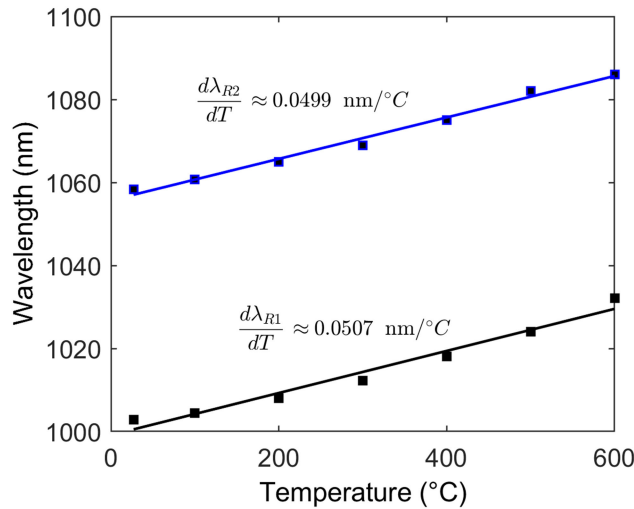
Fig. 6. The resonance wavelengths λ_{R1} and λ_{R2} of the symmetric LPFG versus temperature.
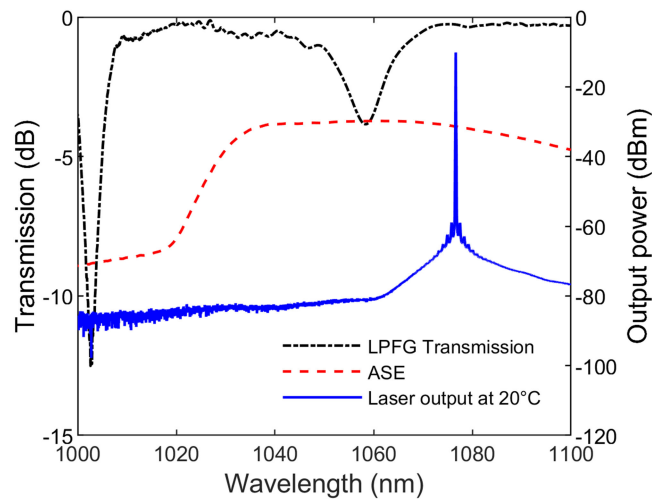

Fig. 7. The transmission spectrum of symmetric LPFG (black), the laser output power at single emission regime (blue), and the doped fiber spectrum (red line). The WSF was set at 20°C (room temperature).

wavelength λ_{R2} is used, avoiding the laser to emit at lower wavelengths. The symmetrical LPFG as WSF allows to alleviate the mode competition and mode hopping effect. Hence, a highly stable performance of the laser is expected [17].

We adjusted the polarization state until the emission of the switchable YDFL was reduced enough to generates a single-line emission centered at 1076.64 nm, presenting an SMSR of 49 dB, and achieving a narrow linewidth of 0.04 nm (see Fig. 8). Besides, to validate the laser stability, its spectrum was scanned repeatedly for 60 min at intervals of 5 min (Fig. 9). The output peak power variation was lower than 0.14 dB, and the wavelength remains unchanged at 1076.64 nm, as it is depicted in Fig. 10. These results indicate not only a high monochromaticity of the laser, but also high stability during all the 60 min of scanning time. Here it is important to point out that, with the change of the polarization state in the cavity via changing achieving by the polarization controller (PC), the variation of transmissions/losses at different wavelengths differs, which result in the selective oscillation at the less loss wavelengths [55]. Hence, when the PC is adjusted, the
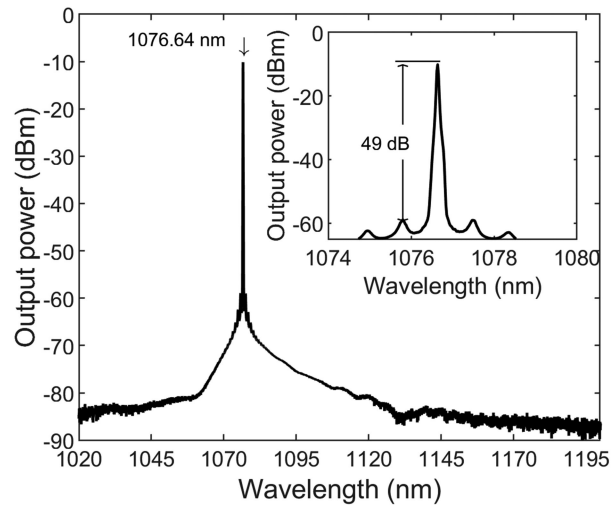
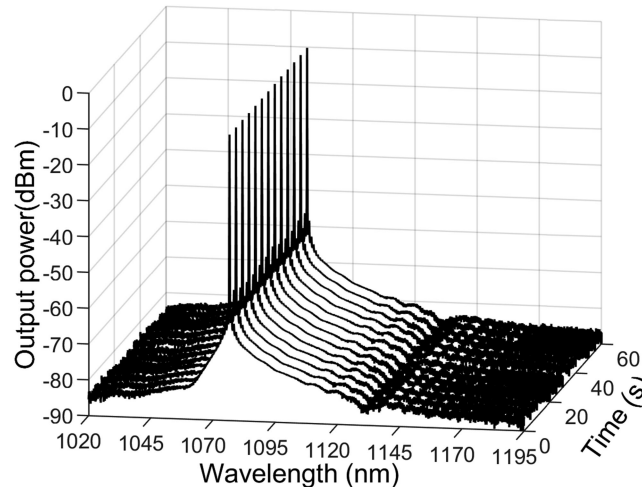Fig. 8. The output power of single laser emission.

Fig. 9. Stability of the single laser emission in 60 min of scan time, output spectra every 5 minutes.

polarization state shifts the symmetric coupling mode and as a result, the resonant wavelength of the LPFG is changed.

4.2 Dual Laser Emission

Upon changing the polarization state of the laser at room temperature, two emission lines were obtained at $\lambda_1 =$ 1075.52 nm and $\lambda_2 =$ 1076.26 nm (Fig. 11) with 3-dB linewidths of 0.09 y 0.28 nm, respectively. The spectral separation between these two lines could be varied by finely adjusting the polarization controller. During the tuning process, there is a point where the two lines overlap in wavelength, producing a single line emission.

Moreover, for the dual laser case the SMSR is 30.4 and 37 dB, respectively. Next, the stability of our proposed laser system at room temperature was scanned every 5 minutes for 45 min (Fig. 12).

For this dual emission case Fig. 13 shows the output power (left axis). The variations at the first five minutes for the emission located at λ_1 and λ_2 were ~0.38 dB ($P_{\lambda 1}$, black squares) and 0.1 dB ($P_{\lambda 2}$, blue square), respectively. On the other hand, λ_1 and λ_2 on the right axis had variations of
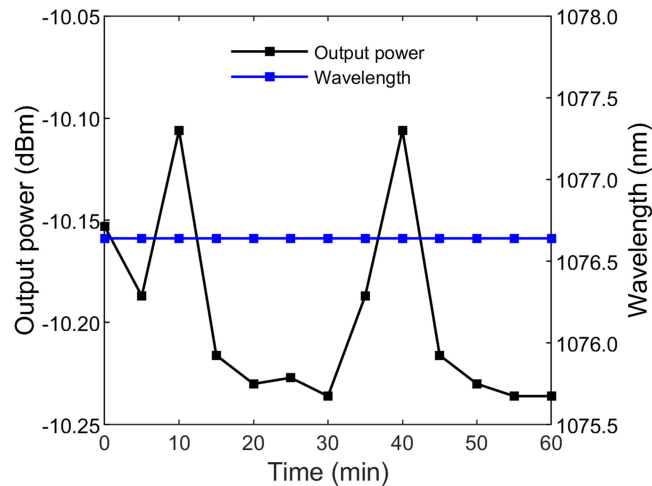
Fig. 10. Output peak power (left side, black line) with maximum output power variation of ∼0.14 dB, and wavelength stability (right side, blue line) over 60 min of scan time (every 5 minutes).
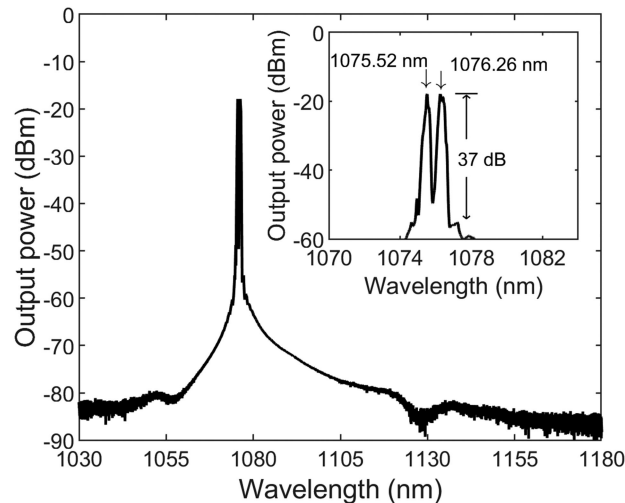

Fig. 11. The output power of laser emitting two beams centered at $\lambda_1 = 1075.52$ nm and $\lambda_2 = 1076.26$ nm.

0.01 nm (λ_1, black triangles) y 0.12 nm (λ_2, blue triangles), respectively, being negligible the rest of the scan time. Therefore, the wavelength and power stability are entirely satisfactory.

The output power variations of the dual line emission can be induced by the raise in the cavity losses due to room temperature fluctuations [19], or by the gain competition between the same wavelength emissions [37]. To obtain more emission lines, changes in the wavelength-dependent loss function can be obtained by operating on the LPFG. When the PC is adjusted, the polarization state shifts the symmetric coupling mode and as a result, the resonant wavelength of the LPFG changes.

4.3 Switchable State Under Temperature Parameter

It is necessary to take into account the changes in wavelength-dependent loss of the symmetrical LPFG as a function of temperature, to achieve the switchable multi-wavelength operation of the
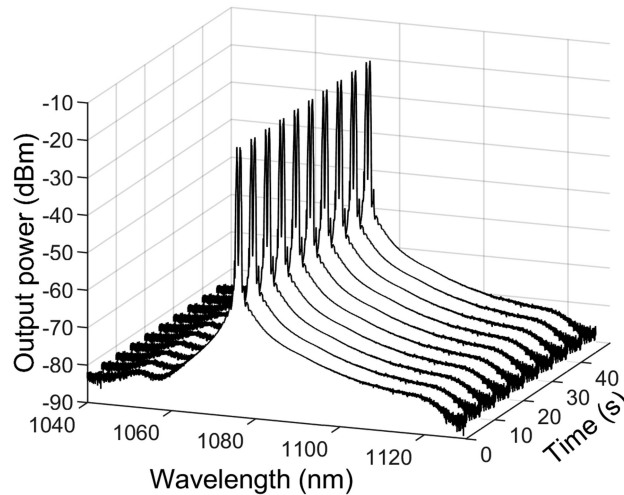
Fig. 12. Stability of dual emission over 45 min of scan time, spectra every 5 minutes.
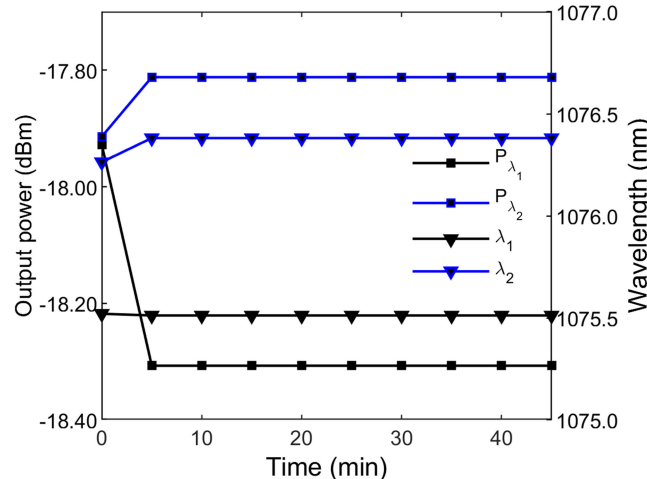

Fig. 13. Output peak power and wavelength stability of dual emission, over 45 min of scan time (every 5 minutes).

YDFL. The symmetrical LPFG was attached to an aluminum plate mounted directly on an electric heater controlled by a PID. Before taking the output power measurement, we waited at least 10 minutes at each temperature to be sure that the temperature was stable.

In Fig. 14 the laser emission and the amplified transmission of the LPFG for temperatures of 27, 50 and 100°C (black, blue, and red lines, respectively) is shown. The wavelength emissions at 27°C are 1041.08 and 1042.06 nm (black line), achieving a SMSR of ~43 dB, and a fine linewidth of ~0.039 nm. When the temperature is increased to 50°C, five beams are generated at 1040.42, 1042.102, 1041.22, 1042.95 and 1043.82 nm (blue line). When temperature reaches 100°C, two beams are observed at 1041.08, and 1042.8 nm (red line). In the transmission spectrum of the LPFG, between the resonant wavelengths λ_{R1} and λ_{R2}, there are low-amplitude side lobes which modify the net gain of the cavity, and we observe that the laser emissions might correspond to these side lobes in the grating transmission. This effect might be produced by the insertion loss due to the accumulated MFD along the LPFG [62]. The shift of the LPFG transmission toward longer wavelengths is produced by the increment the temperature induces on the effective index
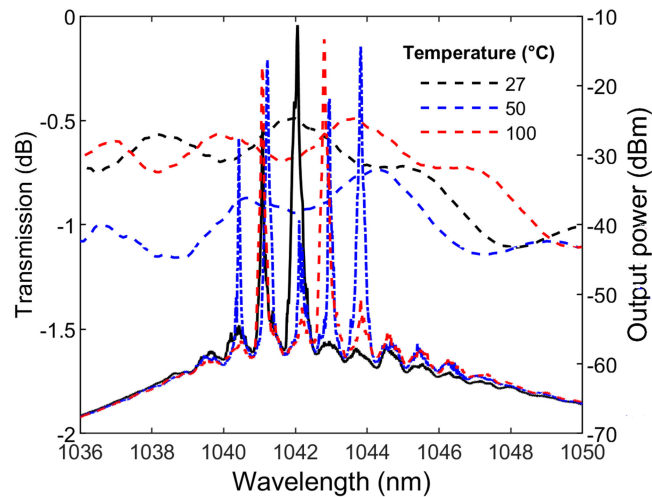
Fig. 14. Laser emission and the amplified transmission of the LPFG at 27, 50, and 100°C.
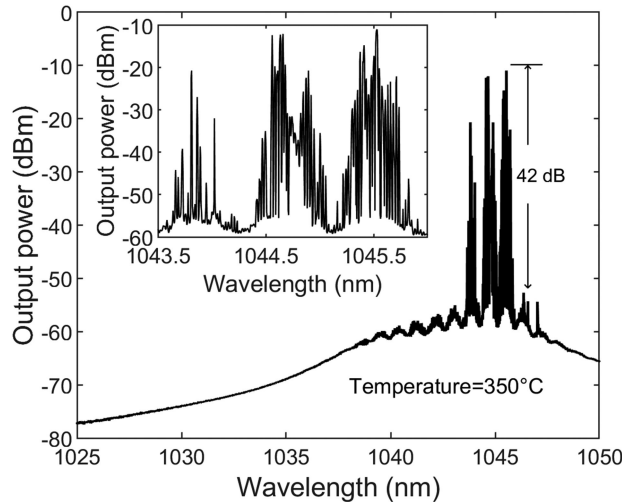

Fig. 15. Multi-wavelength laser emission at 350°C.

difference and is observed along all the temperature experiments. As was mentioned previously, the shift of the LPFG transmission toward longer wavelengths is produced by the increment the temperature induces on the effective index difference. This effect is observed along all the temperature experiments.

Increasing the temperature toward 350°C, multiple emission lines around 1045.53 nm were observed (Fig. 15). This can be explained because the wavelengths between 1040 and 1060 nm correspond to the higher gain for the ytterbium-doped fiber ASE, and for this temperature there are not resonant wavelength suppressing the modal competition in this region. The SMSR and linewidth reached were ∼42 dB and 0.016 nm, respectively.

Fig. 16 shows the case for a temperature of 600°C. Here, one line centered at 1039.2 nm with linewidth of 0.021 nm and SMSR∼42 dB was observed. The laser emission at 600°C corresponds to the lateral right lobe of $\lambda_{R1} =$ 1032.1 nm at 600°C (black line). Specifically, the emissions from 1040 to 1044 nm were suppressed, due to the soft depth observed in the transmission of LPFG. At longer wavelengths, multiple lines were observed around 1046 nm.
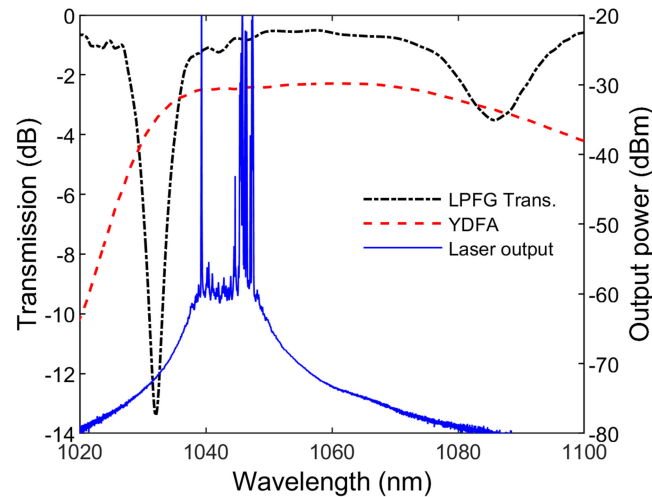
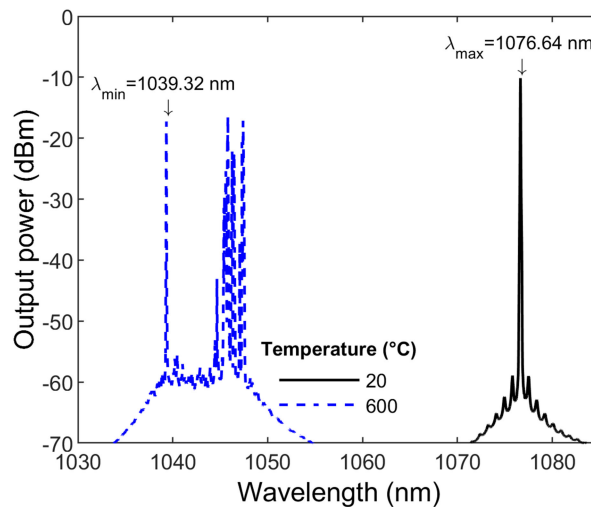Fig. 16. Multiwavelength laser emission and transmission of the LPFG at 600°C.

Fig. 17. Wavelength emission range, from λ_{min} = 1039.32 nm (600°C) to λ_{max} = 1076.64 nm at room temperature (20°C).

To summarize, we have proven the switchable operation of the proposed laser, by changing the temperature on the symmetrical LPFG, from λ_{min}= 1039.32 nm at 600°C, to λ_{max}= 1076.64 nm at room temperature (20°C). (Fig. 17).

The noticeable performance at high temperatures can be explained by the high thermal expansion [72] produced by the diffusion of the dopant and the thermal expansion of the core symmetrical LPFG, due to its fabrication [5], [60]. In fact, for even higher values of temperature (around 750°C) of the symmetrical LPGF, new groups of emission lines were generated in a different wavelength range, nevertheless, the SMSR observed is not high enough. To obtain more emission lines, the wavelength-dependent loss of the LPFG must be controlled. However, it is expected that increasing the number of emissions can affect the laser stability, due to the modal competence in the ytterbium-doped fiber.

These multiple lines might be controlled using a WSF with more resonant wavelengths at these regions for higher temperatures, alleviating the mode competition and mode hopping effect.
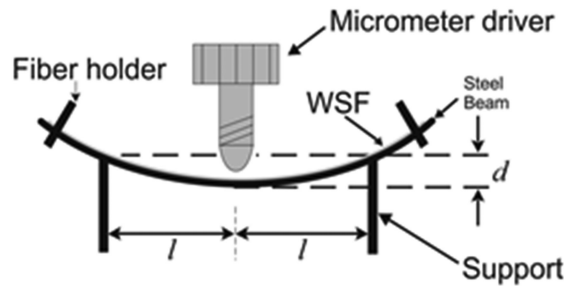
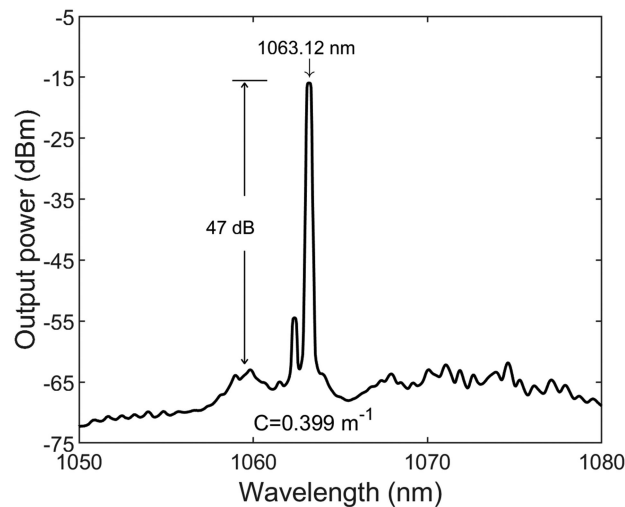Fig. 18. Schematic diagram of the mechanism used to change the curvature radius.

Fig. 19. YDFL single-laser output spectrum for curvature value of 0.399 m^{-1}.

4.4 Switchable State Under Curvature Parameter

In addition, we performed the switching operation of the YDFL under curvature tests on the symmetrical LPFG. To measure the curvature response of the fiber laser, the symmetrical LPFG was fixed over two supports, and was bent it by using a micrometer screw as it can be seen in Fig. 18. The WSF curvature is given by (4):

$$C = \frac{1}{R} = \frac{2d}{(d^2 + l^2)} \tag{4}$$

Where R is the curvature radius, d is the displacement measured at the strip center, and l is half the distance between the two supports [5].

When, at room temperature, the symmetrical LPFG is straight each notch is associated with the coupling of the fundamental core mode LP0m with the cladding modes with the same azimuthal symmetry LP0m [60]. The LPFG was bent to curvature values from 0 to 0.620 m^{-1}. Therefore, the resonance wavelengths λ_R shifts to longer wavelengths, due to changes in the effective refractive index distribution of cladding modes and fundamental core mode caused by the bending strain [5].

The WSF was bent until the linewidth of the laser was reduced enough to obtain single emission. Here, at C = 0.399 m^{-1}, the single emission laser was centered at 1063.12 nm (See Fig. 19). The SMSR reached was 47 dB and a 3-dB linewidth of 0.26 nm was achieved.

When the curvature radius was changed from C = 0.399 m^{-1} (Fig. 20, black line) to C = 0.532 m^{-1} (Fig. 20, blue line), the single-laser emission was tuned from 1063.12 nm to
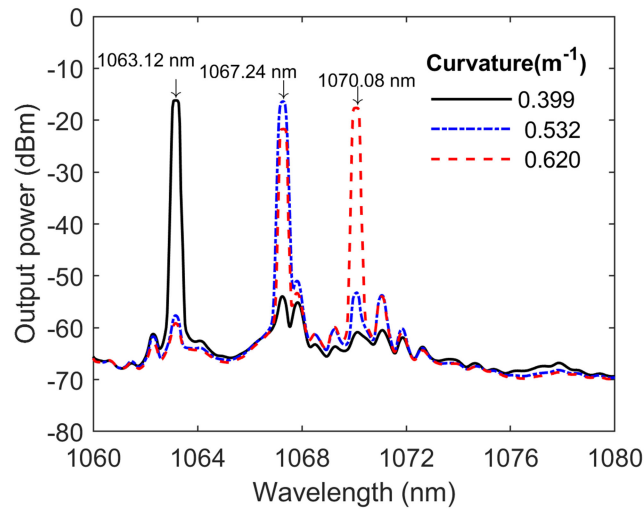
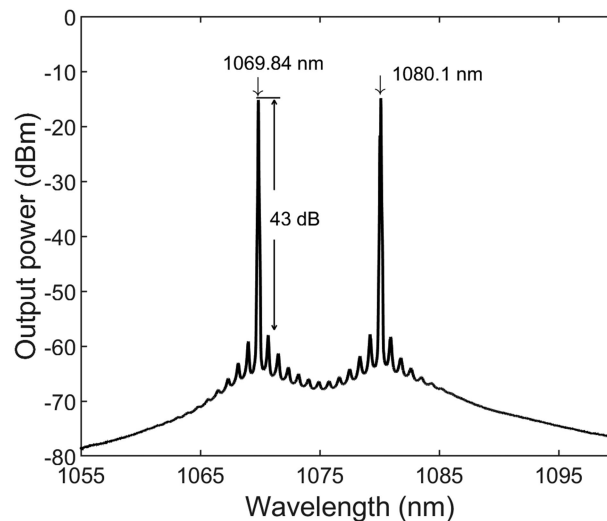Fig. 20. Tuning of one of the laser emissions and begin of the double emission.

Fig. 21. Dual-line output spectrum fiber laser emitted at LPFG bending at C = 0.709 m-1.

1067.24 nm with a SMSR of 47 dB and a 3-dB linewidth of 0.27 nm. After the curvature radius is increased to C = 0.620 m^{-1}, the laser produces a two-line emissions (Fig. 20, red line). One of them centered at $\lambda_1 = 1067.24$ nm, matching with the single emission corresponding to C = 0.532 m^{-1}, and the other one centered at $\lambda_2 = 1070.08$ nm. The room temperature and the PC remains without changes along all the experiment, achieving a switchable laser from one to two lines, only by adjusting the curvature.

The dual-wavelength laser was obtained by increasing the curvature radius of the WSF to C = 0.709 m^{-1} (Fig. 21). Here, narrow 3-dB linewidths of 0.04 and 0.03 nm centered at $\lambda_1 = 1069.84$ nm, and $\lambda_2 = 1080.1$ nm, respectively, and an SMSR of 43 dB were obtained. In this case it is important to comment that during the bending process there is a certain point where the two lines overlap, producing single-line emission. We can understand these results considering that when the symmetrical LPFG is bent, the fiber and its refractive index profile change, breaking the cladding-mode symmetry and promoting the coupling of the fundamental mode to higher modes
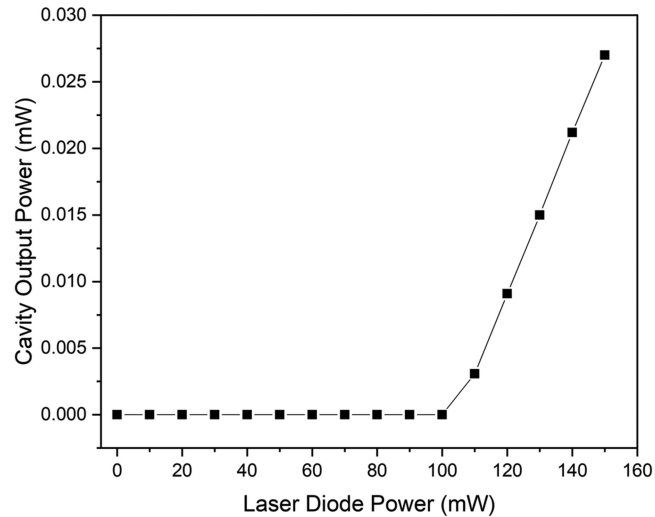
Fig. 22. Slope laser efficiency. The emission is centered at λ = 1076.64 nm.

TABLE 1
Comparison of the Performance of the Switchable Multi-Wavelength YDFL Reported

Ref	WSF	SMSR (dB)	Linewidth (nm)	Output power fluctuation (dB)	Operation range (nm)
[51]	AWG-OCS	60	0.15	0.47	1026 - 1038
[53]	MZI	53	0.01	0.6	1035 - 1050
[30]	FBG	52	0.1	-	1029 - 1040
[16]	PC-PDI	50	0.02	2	1074 - 1090
[31]	SI	44	0.1	0.94	1024 - 1042
[52]	MZI	40	0.07	1	1028 - 1033
[42]	LPFG	40	1	-	1080 - 1100
[56]	LPFG	32	1	Long-term	1080-1100
This paper	LPFG	49	0.04	0.14	1038 - 1080

[5]. Under this consideration, some modes with higher-order azimuthal symmetry might be excited, as is reported in [59]. The YDFL proposed in this work can be switched to single-wavelength or dual-wavelength lasing output acting on the curvature parameter of the LPFG thanks the low PDL of the symmetrical LPFG. The room temperature and the PC remains without changes along all the experiment, achieving a highly stable emission.

To investigate the efficiency of the ring cavity fiber laser, we adjusted the polarization state until the homogeneous linewidth of YDFL was reduced enough to obtain single laser emission. Fig. 22 depicts the output power of the ring cavity laser against the laser diode output power. The laser

efficiency slope was 0.028% with R^2 of 0.993, for laser diode pump power from 200 to 150 mW. This low laser efficiency reported might be produced because in some ytterbium-doped silica fibers, the excited state lifetime of a fraction of the Yb-ions is quenched to a very small value, especially if the pump power is wavelength is around 976 nm, degrading seriously the performance of Yb-doped lasers and amplifiers [73]. Moreover, the attenuation due to absorption of the pump light along the active medium might be high, due the core-pumping used in the experimental scheme. For this reason, the cladding pump is recommended, since only a fraction of the pump field overlaps with the doped core [74]. Additionally, the efficiency, threshold, and maximum output power depend on the fraction power that is outcoupled from the laser cavity. In our case, the available coupler was 90:10. However, a higher ratio such as 99:1 could increase the feedback into the cavity, obtaining eventually a higher output power.

Finally, a performance comparison of our reported laser with other references about switchable YDFLs is made in Table 1.

Here, it can be noticed significant improvements in the power and wavelength stability because of the symmetric LPFG used as WSF. Moreover, several features highly desirable, such as high SMSR, narrow linewidth, and wider switchable operation range by heating or bending the LPFG are achieved.

5. Conclusion

A stable switchable multi-wavelength ytterbium-doped fiber laser was manufactured using a symmetrical LPFG as WSF. The proposed laser can emit a single stable wavelength with an SMSR of 49 dB, and a linewidth of about 0.04 nm during 60 minutes of continuous operation. Furthermore, this YDFL can be switched by changing the temperature, as well as the curvature of the symmetrical LPFG. The proposed laser has several advantages, such as controllability under both high-temperature or curvature conditions, higher SMSR, the narrow linewidth of the output power, stable single and dual-wavelength output powers, and the simple configuration of switchable YDFL. Finally, this laser can be used potentially in different applications, such as biomedical technology, sensing, spectroscopy, dense wavelength-division multiplexing, optical communications, and microwave photonics systems, since its easily switchable wavelength, as well as the cost-effective and repeatable fabrication technique of the symmetrical LPFG used as WSF.

Acknowledgment

References

[1] V. Balaswamy, S. Aparanji, G. Chayran, and V. R. Supradeepa, "High-power, independently wavelength, power, and linewidth tunable ytterbium fiber laser," *IEEE Photon. Technol. Lett.*, vol. 31, no. 8, pp. 583–586, Apr. 2019, doi: 10.1109/lpt.2019.2901504.

[2] R. Royon, J. Lhermite, L. Sarger, and E. Cormier, "High power, continuous-wave ytterbium-doped fiber laser tunable from 976 to 1120 nm," *Opt. Exp.*, vol. 21, no. 11, pp. 13818–13823, Jun. 2013, doi: 10.1364/oe.21.013818.

[3] S. Fu, L. Si, Z. Guo, S. Yuan, Y. Zhao, and X. Dong, "Switchable multiwavelength ytterbium-doped double-clad fiber laser based on a multimode fiber grating," *Appl. Opt.*, vol. 46, no. 17, pp. 3579–3582, Jun. 2007, doi: 10.1364/ao.46.003579.

[4] S. Baek, S. Roh, Y. Jeong, and B. Lee, "Experimental demonstration of enhancing pump absorption rate in cladding-pumped ytterbium-doped fiber lasers using pump-coupling long-period fiber gratings," *IEEE Photon. Technol. Lett.*, vol. 18, no. 5, pp. 700–702, Mar. 2006, doi: 10.1109/lpt.2006.871158.

[5] J. A. Martin-Vela *et al.*, "Curvature sensing setup based on a fiber laser and a long-period fiber grating," *IEEE Photon. Technol. Lett.*, vol. 31, no. 15, pp. 1265–1268, Aug. 2019, doi: 10.1109/lpt.2019.2924847.

[6] H. Ahmad, and M. Dernaika, "Stabilized single longitudinal mode fibre ring laser based on an inline dual taper Mach Zehnder interferometer filter coated with graphene oxide," *Opt. Commun.*, vol. 341, pp. 140–146, 2015, doi: 10.1016/j.optcom.2014.12.024.

[7] Y. Zhou, P. C. Chui, and K. K. Y. Wong, "Multiwavelength single-longitudinal-mode ytterbium-doped fiber laser," *IEEE Photon. Technol. Lett.*, vol. 25, no. 4, pp. 385–388, Feb. 2013, doi: 10.1109/lpt.2013.2238917.

[8] H. Ahmad, M. A. M. Salim, S. R. Azzuhri, M. F. Jaddoa, and S. W. Harun, "Tunable dual-wavelength ytterbium-doped fiber laser using a strain technique on microfiber Mach–Zehnder interferometer," *Appl. Opt.*, vol. 55, no. 4, pp. 778–782, Feb. 2016, doi: 10.1364/ao.55.000778.

[9] W. Yang, Y. Liu, L. Xiao, and Z. Yang, "Wavelength-tunable erbium-doped fiber ring laser employing an acousto-optic filter," *J. Lightw. Technol.*, vol. 28, no. 1, pp. 118–122, Jan. 2010, doi: 10.1109/jlt.2009.2037595.

[10] Y. W. Lee, and B. Lee, "Wavelength-switchable erbium-doped fiber ring laser using spectral polarization-dependent loss element," *IEEE Photon. Technol. Lett.*, vol. 15, no. 6, pp. 795–797, Jun. 2003, doi: 10.1109/lpt.2003.811347.

[11] W. G. Chen *et al.*, "Switchable multi-wavelength fiber ring laser based on a compact in-fiber mach-zehnder interferometer with photonic crystal fiber," *Laser Phys.*, vol. 19, no. 11, pp. 2115–2119, Nov. 2009, doi: 10.1134/s1054660x09210026.

[12] H. Ahmad *et al.*, "Compact L-band switchable dual wavelength SOA based on linear cavity fiber laser," *Optik (Stuttg),* vol. 182, pp. 37–41, Apr. 2019, doi: 10.1016/j.ijleo.2019.01.003.

[13] Y. W. Zhou, G. Y. Sun, and A. P. Luo, "Optically tunable multiwavelength fiber laser based on a Mach-Zehnder comb filter incorporating ytterbium-doped fibers," *Laser Phys.,* vol. 28, no. 1, p. 01505 (5pp), Dec. 2018, doi: 10.1088/1555-6611/aa8add.

[14] M. R. K. Soltanian, H. Ahmad, A. Khodaie, I. S. Amiri, M. F. Ismail, and S. W. Harun, "A stable dual-wavelength thulium-doped fiber laser at 1.9 μ 1/4m using photonic crystal fiber," *Sci. Rep.*, vol. 5, p. 14537 (8pp), Oct. 2015, doi: 10.1038/srep14537.

[15] F. Yin, S. Yang, H. Chen, M. Chen, and S. Xie, "60-nm-wide tunable single-longitudinal-mode ytterbium fiber laser with passive multiple-ring cavity," *IEEE Photon. Technol. Lett.*, vol. 23, no. 22, pp. 1658–1660, Nov. 2011, doi: 10.1109/lpt.2011.2166112.

[16] Y. Zhang, Y. Yang, K. Song, and M. Lv, "Tunable and switchable multi- wavelength ytterbium-doped fiber laser based on nonlinear polarization," in *Proc. SPIE 11333, AOPC 2019: Adv. Laser Mater. Laser Technol.*, no. 11333J, pp. 1–6, Dec. 2019, doi: 10.1117/12.2548127.

[17] M. Bianchetti *et al.*, "Switchable multi-wavelength laser based on a core-offset Mach-Zehnder interferometer with non-zero dispersion-shifted fiber," *Opt. Laser Technol.*, vol. 104, pp. 49–55, 2018, doi: 10.1016/j.optlastec.2018.02.012.

[18] J. M. Estudillo-Ayala *et al.*, "Multi-wavelength fiber laser based on a fiber Fabry–Perot interferometer," *Appl. Phys. B Lasers Opt.*, vol. 121, no. 4, pp. 407–412, Nov. 2015, doi: 10.1007/s00340-015-6265-z.

[19] Y. Qi *et al.*, "Wavelength-switchable fiber laser based on few-mode fiber filter with core-offset structure," *Opt. Laser Technol.*, vol. 81, pp. 26–32, 2016, doi: 10.1016/j.optlastec.2016.01.022.

[20] J. M. Sierra-Hernandez *et al.*, "A tunable multi-wavelength erbium doped fiber laser based on a Mach-Zehnder interferometer and photonic crystal fiber," *Laser Phys.,* vol. 23, no. 12, pp. 125103 (6pp), Nov. 2013, doi: 10.1088/1054-660x/23/12/125103.

[21] C.-R. Hu *et al.*, "Stimulated raman scattering imaging by continuous-wave laser excitation," *Opt. Lett.*, vol. 38, no. 9, pp. 1479–1481, May 2013, doi: 10.1364/ol.38.001479.

[22] X. Zhang, W. Lee, and X. Fan, "Bio-switchable optofluidic lasers based on DNA Holliday junctions," *Lab Chip*, vol. 12, no. 19, pp. 3673–3675, 2012, doi: 10.1039/c2lc40183e.

[23] J. M. Sierra-Hernandez *et al.*, "Torsion sensing setup based on a three beam path Mach–Zehnder interferometer," *Microw. Opt. Technol. Lett.*, vol. 57, no. 8, pp. 1857–1860, Aug. 2015, doi: 10.1002/mop.26128.

[24] G. Anzueto-Sánchez, A. Martínez-Rios, and J. Castrellon-Uribe, "Tuning and wavelength switching erbium-doped fiber ring lasers by controlled bending in arc-induced long-period fiber gratings," *Opt. Fiber Technol.*, vol. 18, no. 6, pp. 513–517, 2012, doi: 10.1016/j.yofte.2012.08.004.

[25] A. J. Metcalf *et al.*, "Stellar spectroscopy in the near-infrared with a laser frequency comb," *Optica*, vol. 6, no. 2, pp. 233–239, Feb. 2019, doi: 10.1364/optica.6.000233.

[26] D. Leandro, V. DeMiguel Soto, R. A. Perez-Herrera, M. Bravo Acha, and M. Lopez-Amo, "Random DFB fiber laser for remote (200 km) sensor monitoring using hybrid WDM/TDM," *J. Lightw. Technol.*, vol. 34, no. 19, pp. 4430–4436, 2016, doi: 10.1109/jlt.2016.2547868.

[27] D. G. Mina, J. W. Haus, A. Chong, A. Khanolkar, A. Sarangan, and K. Hansen, "Bi-tapered fiber sensor using visible to near infrared light," *Sensors Actuators, A Phys,* vol. 263, pp. 285–290, Jun. 2017, doi: 10.1016/j.sna.2017.06.017.

[28] H. Fu, D. Chen, and Z. Cai, "Fiber sensor systems based on fiber laser and microwave photonic technologies," *Sensors*, vol. 12, no. 5, pp. 5395–5419, Apr. 2012, doi: 10.3390/s120505395.

[29] Q. Zhao *et al.*, "Switchable multi-wavelength erbium-doped fiber laser with adjustable wavelength interval," *J. Lightw. Technol.*, vol. 37, no. 15, pp. 3784–3790, Aug. 2019, doi: 10.1109/jlt.2019.2920840.

[30] H. Wang, Y. G. Li, X. D. Chen, B. Huang, F. Y. Lu, and K. C. Lu, "Highly efficient dual-wavelength ytterbium-doped fiber linear cavity laser based on cascaded fiber bragg gratings," *Laser Phys.,* vol. 19, no. 6, pp. 1257–1262, Jun. 2009, doi: 10.1134/s1054660x09060139.

[31] X. Liu, S. Lou, Z. Tang, Y. Zhou, H. Jia, and P. Sun, "Tunable dual-wavelength ytterbium-doped fiber ring laser based on a sagnac interferometer," *Opt. Laser Technol.*, vol. 116, pp. 37–42, Mar. 2019, doi: 10.1016/j.optlastec.2019.03.006.

[32] X. Ma, S. Luo, and D. Chen, "Switchable and tunable thulium-doped fiber laser incorporating a sagnac loop mirror," *Appl. Opt.*, vol. 53, no. 20, pp. 4382–4385, Jul. 2014, doi: 10.1364/ao.53.004382.

[33] X. Liu, L. Zhan, S. Luo, Y. Wang, and Q. Shen, "Individually switchable and widely tunable multiwavelength erbium-doped fiber laser based on cascaded mismatching long-period fiber gratings," *J. Lightw. Technol.*, vol. 29, no. 21, pp. 3319–3326, Nov. 2011, doi: 10.1109/jlt.2011.2168386.

[34] M. R. A. Moghaddam *et al.*, "Multiwavelength ytterbium-doped fiber ring laser," *Microw. Opt. Technol. Lett.*, vol. 51, no. 10, pp. 2511–2512, Oct. 2009, doi: 10.1002/mop.24605.

[35] J. A. Martin-Vela *et al.*, "Switchable and tunable multi-wavelength fiber laser based on a core-offset aluminum coated Mach-Zehnder interferometer," *Opt. Laser Technol.*, vol. 125, Art. no. 106039, 2020, doi: 10.1016/j.optlastec.2019.106039.

[36] A. A. Castillo-Guzmán *et al.*, "In-fiber Mach-Zehnder interferometer based on a Nd-doped double-clad fiber for switchable single and dual-wavelength EDF laser application," *Laser Phys.,* vol. 27, no. 5, p. 055102 (6pp), Mar. 2017, doi: 10.1088/1555-6611/aa6851.

[37] H. Ahmad, and A. A. Jasim, "Stable C-band fiber laser with switchable multi-wavelength output using coupled microfiber Mach-Zehnder interferometer," *Opt. Fiber Technol.*, vol. 36, pp. 105–114, 2017, doi: 10.1016/j.yofte.2017.03.003.

[38] O. M. Kharraz, A. B. B. Mohammad, H. Ahmad, and A. A. Jasim, "Performance enhancement of multi-wavelength generations based on SOAs with a microfiber Mach–Zehnder interferometer," *Laser Phys.,* vol. 27, no. 7, p. 075101, Jul. 2017, doi: 10.1088/1555-6611/aa6e40.

[39] A. Camarillo-Aviles *et al.*, "Stable multi-wavelength thulium-doped all-fiber laser incorporating a multi-cavity Fabry–Perot filter," *IEEE Photon. J.,* vol. 11, no. 6, Dec. 2019, doi: 10.1109/jphot.2019.2949500.

[40] G. Salceda-Delgado *et al.*, "Reconfiguration of the multiwavelength operation of optical fiber ring lasers by the modifiable intra-cavity induced losses of an in-fiber tip probe modal michelson interferometer," *Laser Phys.,* vol. 28, no. 3, pp. 035107 (6pp), Feb. 2018, doi: 10.1088/1555-6611/aaa02e.

[41] X. Luo, T. H. Tuan, T. S. Saini, H. P. T. Nguyen, T. Suzuki, and Y. Ohishi, "Spacing-adjustable multi-wavelength erbium-doped fiber laser using a fiber michelson interferometer," *Appl. Phys. Exp.*, vol. 11, no. 8, pp. 082501 (4pp), Aug. 2018, doi: 10.7567/apex.11.082501.

[42] D. E. Ceballos-Herrera, I. Torres-Gomez, A. Martinez-Rios, G. Anzueto-Sanchez, and Y. Barmenkov, "Single- to three-wavelength switchable ytterbium-doped fiber laser based on intracavity induced loss by a long-period holey fiber grating," *Opt. Laser Technol.*, vol. 43, no. 4, pp. 825–829, 2011, doi: 10.1016/j.optlastec.2010.11.003.

[43] N. S. Shahabuddin *et al.*, "Multi-wavelength ytterbium doped fiber laser based on longitudinal mode interference," *Laser Phys.,* vol. 22, no. 1, pp. 252–255, 2012, doi: 10.1134/s1054660x12010173.

[44] J. Boullet *et al.*, "High power ytterbium-doped rod-type three-level photonic crystal fiber laser," *Opt. Exp.*, vol. 16, no. 22, pp. 17891, Oct. 2008, doi: 10.1364/oe.16.017891.

[45] X. Feng, Y. Liu, S. Fu, S. Yuan, and X. Dong, "Switchable dual-wavelength ytterbium-doped fiber laser based on a few-mode fiber grating," *IEEE Photon. Technol. Lett.*, vol. 16, no. 3, pp. 762–764, Mar. 2004, doi: 10.1109/lpt.2004.823722.

[46] Y. Yasuno *et al.*, "In vivo high-contrast imaging of deep posterior eye by 1-μm swept source optical coherence tomography and scattering optical coherence angiography," *Opt. Exp.,* vol. 15, no. 10, pp. 6121–6139, May 2007, doi: 10.1364/oe.15.006121.

[47] M. R. A. Moghaddam, S. W. Harun, S. Shahi, K. S. Lim, and H. Ahmad, "Comparisons of multi-wavelength oscillations using sagnac loop mirror and Mach-Zehnder interferometer for ytterbium doped fiber lasers," *Laser Phys.,* vol. 20, no. 2, pp. 516–521, 2010, doi: 10.1134/s1054660x10030138.

[48] H. Han, X. Li, S. Zhang, and M. Han, "Precise wavelength control of yb-doped fiber laser using fused tapered fiber technology," *J. Lightw. Technol.*, vol. 37, no. 3, pp. 715–721, 2019, doi: 10.1109/jlt.2018.2877802.

[49] S. W. Harun *et al.*, "Diode-pumped 1028 nm Ytterbium-doped fiber laser with near 90% slope efficiency," *Laser Phys.,* vol. 20, no. 3, pp. 656–660, Mar. 2010, doi: 10.1134/s1054660x10050051.

[50] R. Paschotta, J. Nilsson, A. C. Tropper, and D. C. Hanna, "Ytterbium-doped fiber amplifiers," *IEEE J. Quantum Electron.*, vol. 33, no. 7, pp. 1049–1056, Jul. 1997, doi: 10.1109/3.594865.

[51] H. Ahmad, A. A. Latif, S. F. Norizan, M. Z. Zulkifli, and S. W. Harun, "Flat and compact switchable dual wavelength output at 1060nm from ytterbium doped fiber laser with an AWG as a wavelength selector," *Opt. Laser Technol.*, vol. 43, no. 3, pp. 550–554, 2011, doi: 10.1016/j.optlastec.2010.07.013.

[52] A. Guzman-Castillo *et al.*, "Ytterbium fiber laser based on a three beam optical path Mach-Zehnder interferometer," *IEEE Photon. Technol. Lett.*, vol. 28, no. 23, pp. 2678–2771, Dec. 2016, doi: 10.1109/lpt.2016.2616466.

[53] A. S. Zulkhairi *et al.*, "Switchable multiwavelength ytterbium-doped fiber laser using a non-adiabatic microfiber interferometer," *Laser Phys.,* vol. 27, no. 5, pp. 055104 (6 pp), Apr. 2017, doi: 10.1088/1555-6611/aa6587.

[54] A. Martinez-Rios, D. Monzon-Hernandez, I. Torres-Gomez, and G. Salceda-Delgado, "Long period fibre gratings," in *Fiber Optic Sensors*, M. Yasin, Ed. InTech, 2012, pp. 275–294.

[55] S. X. Liu, C. H. Wang, X. J. Zhu, C. X. Bu, and G. J. Zhang, "Arbitrarily switchable multi-wavelength Yb-doped fiber lasers with phase-shifted long-period fiber grating," *Laser Phys.,* vol. 22, no. 7, pp. 1260–1264, 2012, doi: 10.1134/s1054660x12070080.

[56] P. Peterka, J. Maria, B. Dussardie, R. Slavík, P. Honzátko, and V. Kubeček, "Long-period fiber grating as wavelength selective element in double-clad Yb-doped fiber-ring lasers," *Laser Phys. Lett.*, vol. 6, no. 10, pp. 732–736, Jul. 2009, doi: 10.1002/lapl.200910067.

[57] Y. Wang, "Review of long period fiber gratings written by CO_2 laser," *J. Appl. Phys.*, vol. 108, no. 8, pp. 081101 (18 pp), Oct. 2010, doi: 10.1063/1.3493111.

[58] S. T. Oh, W. T. Han, U. C. Paek, and Y. Chung, "Azimuthally symmetric long-period fiber gratings fabricated with CO_2 laser," *Microw. Opt. Technol. Lett.*, vol. 41, no. 3, pp. 188–190, 2004, doi: 10.1002/mop.20088.

[59] U. L. Block, V. Dangui, M. J. F. Digonnet, and M. M. Fejer, "Origin of apparent resonance mode splitting in bent long-period fiber gratings," *J. Lightw. Technol.*, vol. 24, no. 2, pp. 1027–1034, Feb. 2006, doi: 10.1109/jlt.2005.862430.

[60] T. E. Porraz-Culebro *et al.*, "Characteristics of LPFGs written by a CO_2-Laser glass processing system," *J. Lightw. Technol.*, vol. 37, no. 4, pp. 1301–1309, Feb. 2019, doi: 10.1109/jlt.2019.2892326.

[61] T. Feng, M. H. Jenkins, F. Yan, and T. K. Gaylord, "Arc fusion splicing effects in large-mode-area single-mode ytterbium-doped fibers," *Appl. Opt.*, vol. 52, no. 32, pp. 7706–7711, Nov. 2013, doi: 10.1364/ao.52.007706.

[62] W. Zheng, "Fabrication of long period fiber gratings with CO_2 laser fusion splicers," in *Proc. 2016 IEEE Optoelectron. Global Conf.*, Sep. 2016, pp. 1–4, doi: 10.1109/ogc.2016.7590487.

[63] M. Kihara, S. Tomita, and M. Matsumoto, "Loss characteristics of thermally diffused expanded core fiber," *IEEE Photon. Technol. Lett.*, vol. 4, no. 12, pp. 1390–1391, Dec. 1992, doi: 10.1109/68.180586.

[64] X. Shen *et al.*, "Manufacturing a long-period grating with periodic thermal diffusion technology on High-NA fiber and its application as a high-temperature sensor," *Sensors*, vol. 18, no. 5, pp. 1475 (10 pp), May 2018, doi: 10.3390/s18051475.

[65] M.-S. Yoon, S. Park, and Y.-G. Han, "Simultaneous measurement of strain and temperature by using a micro-tapered fiber grating," *J. Lightw. Technol.*, vol. 30, no. 8, pp. 1156–1160, Apr. 2012, doi: 10.1109/jlt.2011.2170552.

[66] E. M. Dianov *et al.*, "Thermo-induced long-period fibre gratings," in *IEEE conference publication ECOC*, vol. 97, Sep. 1997, no. 448, pp. 53–56, doi: 10.1049/cp:19971415.

[67] P.-H. Lu, K.-C. Hsu, S.-S. Jyu, and Y. Lai, "Periodically tapered long-period fiber gratings by CO_2 laser heating and tension stretching," in *Tech. Dig. - 15th Optoelectron. Commun. Conf., OECC2010*, Jul. 2010, pp. 626–627.

[68] T. Erdogan, "Fiber grating spectra," *J. Lightw. Technol.*, vol. 15, no. 8, pp. 1277–1294, Aug. 1997, doi: 10.1109/50.618322.

[69] K. Morishita, and A. Kaino, "Adjusting resonance wavelengths of long-period fiber gratings by the glass-structure change," *Appl. Opt.*, vol. 44, no. 24, pp. 5018–5023, Aug. 2005, doi: 10.1364/AO.44.005018.

[70] X. Shu, L. Zhang, and I. Bennion, "Sensitivity characteristics of long-period fiber gratings," *J. Lightw. Technol.*, vol. 20, no. 2, pp. 255–266, Feb. 2002, doi: 10.1109/50.983240.

[71] Y.-J. Kim, U.-C. Paek, and B. H. Lee, "Measurement of refractive-index variation with temperature by use of long-period fiber gratings," *Opt. Lett.*, vol. 27, no. 15, pp. 1297–1299, 2002, doi: 10.1364/ol.27.001297.

[72] Y. Wang, W. Jin, and D. N. Wang, "Unique temperature sensing characteristics of CO_2-laser-notched long-period fiber gratings," *Opt. Lasers Eng.*, vol. 47, no. 10, pp. 1044–1048, Apr. 2009, doi: 10.1016/j.optlaseng.2009.03.005.

[73] R. Paschotta, J. Nilsson, P. R. Barber, J. E. Caplen, A. C. Tropper, and D. C. Hanna, "Lifetime quenching in Yb-doped fibres," *Opt. Commun.*, vol. 136, no. 5–6, pp. 375–378, 1997, doi: 10.1016/S0030-4018(96)00720-1.

[74] A. Iho, M. Söderlund, J. Montiel i Ponsoda, J. Koponen, and S. Honkanen, "Modeling inversion in an ytterbium-doped fiber," in *Proc. SPIE 7212, optical components and materials vl*, Feb. 2009, vol. 7212, pp. 721209, doi: 10.1117/12.807820.